Integral Sliding Mode Surface Based Super-Twisting Combined with Model Predictive Flux Control for LIM Applied to Linear Metro Systems

Abdul Khalique Junejo[1,2], *Senior Member,IEEE*
[1]Electrical Engineering Department, King Fahd University of Petroleum & Minerals (KFUPM), Saudi Arabia
[2]Interdisciplinary Research Center for Sustainable Energy Systems (IRC-SES), KFUPM, Saudi Arabia
e-mails: abdulkhalique.junejo@kfupm.edu.sa

Mohammad A. Abido[1,2], *Senior Member,IEEE*
[1]Electrical Engineering Department, King Fahd University of Petroleum & Minerals (KFUPM), Saudi Arabia
[2]Interdisciplinary Research Center for Sustainable Energy Systems (IRC-SES), KFUPM, Saudi Arabia
e-mails: mabido@kfupm.edu.sa

***Abstract*—This paper presents an integral sliding mode surface-based super-twisting control (ISMS-STC) strategy for speed regulation, integrated with finite set-model predictive flux control (FS-MPFC), aimed at improving the dynamic performance of linear induction motors (LIMs) across their entire speed range. The approach begins with the design of the FS-MPFC method, which mitigates the drawbacks associated with conventional finite set-model predictive thrust control (FS-MPTC), notably the complex tuning of weighting factors and computationally intensive processes. Subsequently, the ISMS-STC technique is developed for the speed loop, leveraging FS-MPFC to deliver rapid transient behaviors and robust tracking capabilities, characterized by reduced thrust and flux ripples. A comprehensive examination of the ISMS-STC-MPFC methodology is undertaken, covering its fundamental design principles, implementation procedures, and stability assessment. Extensive simulations and experimental validations are performed on a 3-kW prototype arc induction motor under startup, varied speed and load conditions to demonstrate the efficacy and advantage of the proposed ISMS-STC-MPFC approach.**

***Index Terms*— Integral sliding mode surface-based super-twisting control (ISMS-STC), finite set-model predictive flux control (FS-MPFC), linear induction machine (LIM), Lyapunov function.**

I. Introduction

Linear induction machines (LIMs) are a promising technology for various industrial applications, particularly light rail transit [1]–[3]. Their advantages include direct thrust generation, a small turning radius, low maintenance costs, fast acceleration/deceleration, reduced noise, and excellent hill-climbing ability [4]. LIMs are theoretically derived from rotary induction machines (RIMs) by cutting and flattening the rotor. To date, 30 commercial metro lines worldwide utilize this technology [5]–[7]. However, LIMs suffer from end effects due to magnetic field distortions at the ends of the primary winding. This phenomenon, which varies with speed, adversely impacts dynamic performance and results in lower efficiency compared to RIMs [8]–[11]. Furthermore, implementing control strategies is more challenging for LIMs than for RIMs since of their highly nonlinear and strongly coupled primary and secondary structures [12]. The two primary control structures for drive systems are field-oriented control (FOC) and direct thrust control (DTC) [13]–[15]. FOC, known for its robust performance, is commonly used in RIM traction drives. In FOC, maintaining a constant rotor flux (*d*-axis current) provides operation under constant torque. Under this condition, the motor torque is proportional to the slip frequency (*q*-axis current). Though, the performance of FOC-based drives can degrade due to parameter variations in the LIM system.

Thus, research has explored the application of indirect FOC, direct FOC, and conventional DTC for LIMs. While viable, indirect and direct FOC exhibit slower dynamic behaviors and require knowledge of numerous parameters. These methods also necessitate the careful tuning of three PI regulators (for speed, thrust, and flux loops) and two Clark transformations for full dynamic operation. In contrast, DTC is often a superior choice for small to medium-power applications requiring fast behavior. DTC for LIMs operates differently from FOC. It directly controls primary flux and thrust in the stationary reference frame. Error signals from flux and thrust comparators are used with a switching table to select the optimal voltage vector. Despite its advantages, conventional DTC has significant drawbacks, including poor thrust and flux control at low speeds, high thrust ripple, high current distortion, acoustic noise, and variable switching frequency caused by the hysteresis comparators [13], [14].

To overcome the limitations of both traditional DTC and FOC, model predictive control (MPC) approaches have gained attention in LIM drive systems. MPC offers benefits such as quick dynamic behavior, online optimization, low current fluctuation, and reduced switching losses [16], [17]. MPC is categorized into two main types: finite-set MPC (FS-MPC) and continuous-set MPC [18]. FS-MPC is further divided into model predictive current control (FS-MPCC) and model predictive thrust control (FS-MPTC) [19]. FS-MPCC can suffer from long computation times, while FS-MPTC requires a weighting factor in its cost function to balance thrust and flux errors, adding complexity to the system design. FS-MPC is well-suited for use with a voltage source inverter (VSI) due to the discrete nature of the inverter's limited switching states. In the FS-MPTC method, the cost function typically evaluates the errors in thrust and flux linkage [18]. The switching vector that minimizes this cost function is selected for each control cycle. To eliminate the need for a weighting factor, recent studies have proposed factor-less cost functions [19]. Some methods modify

979-8-3315-7640-0/25/$31.00 ©2025 IEEE
979-8-3315-8138-1

the flux term with the thrust term, while others optimize the terms in parallel [20]. Although these approaches remove the weighting factor, they can still involve significant computational steps [21]. In this paper, a simplified approach is designed: the thrust error term is entirely removed from the cost function, leaving only the primary flux vector error (in the $\alpha\beta$-frame) as the control variable. This technique is termed finite-set model predictive flux control (FS-MPFC). The conventional control schemes for LIMs typically employ PI controller for the speed loop. Yet, the use of PI regulators in the loop often results in a slow dynamic behavior, steady-state variations, and poor performance under load disturbances. As established in the literature, PI controllers generate significant ripple in flux and thrust behaviors, making them unsuitable for smooth control across the entire operating range of LIM.

Consequently, there is a clear need for more robust control methods to achieve superior performance, particularly during transient conditions. The rapid advancement of modern control technology has led to the application of various sophisticated techniques to LIMs, including adaptive control [21], back-stepping [11], model predictive control [14], intelligent methods [10], and sliding mode control (SMC) [21]. Among these, SMC is particularly suitable due to its simple structure, fast dynamic behavior, and inherent robustness to load disturbances and parameter uncertainties. While SMC offers superior performance over PI control and is widely used in motor drives, it is plagued by the problem of high-frequency chattering. This chattering can be lessened by using higher-order SMC (HOSMC), which is achieved by considering the derivatives of the sliding surface variable [15]. The super-twisting SMC (ST-SMC) algorithm provides a simplified approach to designing a second-order SMC. A key advantage of ST-SMC is that its control law does not require direct information about the derivative of the sliding surface, avoiding the need for discontinuous control signals and resulting in a continuous control action that effectively reduces chattering amplitude. Although ST-SMC is robust against disturbances, it often requires high switching gains to compensate for them, which can, in turn, re-introduce chattering into the system. While ST-SMC represents a significant improvement over conventional SMC by reducing chattering, its transient and steady-state performance still requires further enhancement.

Therefore, an integral sliding mode surface-based super-twisting control (ISMS-STC) strategy is adopted for the speed controller to attain a quicker transient behavior, high tracking precision, and lesser thrust and flux ripple. This combination effectively reduces noise and vibration in the LIM. The rest of manuscript is organized as follows. Section II presents the dynamic modeling of the LIM drive system. The design the FS-MPFC method is detailed in Section III. Section IV describes the design of the ISMS-STC -based speed controller for the FS-MPFC strategy. Comprehensive simulation and experimental results in Sections V and VI demonstrate that the proposed ISMS-STC based FS-MPFC scheme offers robust anti-disturbance capability, quicker convergence, and lesser thrust and flux ripples. Finally, conclusions are presented.

II. Modeling of The LIM Drive Systems

The mathematical model of the LIM is derived from its equivalent circuit in the $\alpha\beta$-axis, as illustrated in Fig. 1 [18]. The corresponding equations are presented under:

The voltage expressions on the $\alpha\beta$-axes are described as

$$u_1 = R_1 i_1 + p\psi_1 - j\omega_1\psi_1 \tag{1}$$

$$u_2 = R_2 i_2 + p\psi_2 - j\omega_{slip}\psi_2 = 0 \tag{2}$$

where $u_1 = u_{1\alpha} + j u_{1\beta}$ and $u_2 = u_{2\alpha} + j u_{2\beta}$ demonstrate the primary and secondary voltages, $i_1 = i_{1\alpha} + j i_{1\beta}$ and $i_2 = i_{2\alpha} + j i_{2\beta}$ display the primary and secondary currents, p denotes the differential operator, $\psi_1 = \psi_{1\alpha} + j\psi_{1\beta}$ and $\psi_2 = \psi_{2\alpha} + j\psi_{2\beta}$ show the primary and secondary flux linkages, and R represents the resistance of the LIM, respectively. Additionally, the $\omega_{slip} = \omega_1$-ω_2 represent the slip angular velocity, where ω_1 and ω_2 are the simultaneous and rotating speeds, distinctly.

The flux expressions on the $\alpha\beta$-axes can be uttered as

$$\psi_1 = L_1 i_1 + L_{meq} i_1 \tag{3}$$

$$\psi_2 = L_2 i_2 + L_{meq} i_2 \tag{4}$$

where L_1 and L_2 are the the primary and secondary inductances, and L_{meq} is the equivalent magnetizing inductance adapted by $f(Q)$ [12]. Electromagnetic thrust is stated as:

$$F_e = (3\pi/2\tau)(\psi_{\alpha 1} i_{\beta 1} - \psi_{\beta 1} i_{\alpha 1}) \tag{5}$$

where τ is the primary polar length. The mechanical dynamics of the LIM is given by:

$$F_e = F_l + (G\dot{v}_r + Hv_r)J \tag{6}$$

where F_l denotes the load thrust the mass, H the viscous friction coefficient, v_r the rotor speed, and J the compensate coefficient of the LIM. To account for longitudinal end effects, the equivalent magnetizing inductance is updated using the correction factor $f(Q)$, following the method in [27].

$$f(Q) = (1 - exp(-Q))/Q \tag{7}$$

$$Q = L_1 R_2 / L_2 v_r \tag{8}$$

The L_1 and L_2 can be expressed as $L_1 = L_{l1} + L_{meq}$ and $L_2 = L_{l2} + L_{meq}$ the primary and secondary inductances, respectively, as determined by the revised magnetizing inductance.

$$L_{meq} = [1 - f(Q)]L_m \tag{9}$$

where L_m is the magnetizing inductance at still.

III. Finite Set Model Predictive Flux Control of LIM

In this part, the finite set-model predictive flux control (FS-MPFC) approach is developed for LIM drive system. The cost function in the conventional finite-Set model predictive thrust control (FS-MPTC) incorporates both thrust and primary flux terms. Since these variables are dissimilar physical units, their direct combination in a single cost function presents an optimization challenge, typically requiring a weighting factor to balance their respective errors.

To address this issue and simultaneously reduce computational burden and minimize thrust/flux ripples, the FS-MPFC method is designed. In FS-MPFC, the cost function is

979-8-3315-8138-1

simplified to utilize only the primary flux linkage for prediction, thereby eliminating the need for a weighting factor entirely. The FS-MPFC strategy retains the same three-step predictive control structure as FS-MPTC for effective control of the LIM drive system. These steps can be given as:

- Step 1: The flux observer is adapted to estimate the primary flux-linkage $\psi_{\alpha\beta 1}(k)$ and secondary flux-linkage $\psi_{\alpha\beta 2}(k)$, as confirmed by

$$\psi_{\alpha 1}(k) = \psi_{\alpha 1}(k-1) + T_s\left(u_{\alpha 1}(k) - R_1 i_{\alpha 1}(k)\right) \tag{10}$$

$$\psi_{\beta 1}(k) = \psi_{\beta 1}(k-1) + T_s\left(u_{\beta 1}(k) - R_1 i_{\beta 1}(k)\right) \tag{11}$$

$$\psi_{\alpha 2}(k) = \frac{L_b}{L_{meq}}\psi_{\alpha 1}(k) + \left(L_{meq} - \frac{L_1 L_2}{L_{meq}}\right) i_{\alpha 1}(k) \tag{12}$$

$$\psi_{\beta 2}(k) = \frac{L_2}{L_{meq}}\psi_{\beta 1}(k) + \left(L_{meq} - \frac{L_1 L_2}{L_{meq}}\right) i_{\beta 1}(k) \tag{13}$$

- Step 2: The first-order Euler method is adopted to predict the primary and secondary flux linkages, which are illustrated as follows:

$$\psi_{\alpha\beta 1}(k) = \psi_{\alpha\beta 1}(k-1) + T_s\left(u_{\alpha\beta 1}(k) - R_1 i_{\alpha\beta 1}(k)\right) \tag{14}$$

$$\psi_{\alpha\beta 2}(k) = \frac{L_s}{L_{meq}}\psi_{\alpha\beta 2}(k) + \left(L_{meq} - \frac{L_1 L_2}{L_{meq}}\right) i_{\alpha\beta 1}(k) \tag{15}$$

Again, same procedure can be adopted to predict the primary flux linkage $\psi_{\alpha\beta 1}(k+1)$, which is given by

$$\psi_{\alpha\beta 1}(k+1) = \psi_{\alpha\beta 1}(k) + T_s\left(u_{\alpha\beta 1}(k) - R_a i_{\alpha\beta 1}(k)\right) \tag{16}$$

- Step 3: The cost function's design for the FS-MPFC is described by

$$J = (\left|\psi_{\alpha 1}^* - \psi_{\alpha 1}(\text{k+1})\right|)^2 + (\left|\psi_{\beta 1}^* - \psi_{\beta 1}(\text{k+1})\right|)^2 \tag{17}$$

It can be noted from (17) that the cost function has only primary flux linkage error without weighting factor. The primary flux is commonly selected as ψ_1^*.

$$\left|\psi_1^*\right| = \psi_1^* \tag{18}$$

The maximum thrust of the LIM can be attained when primary current reached at nominal value. The secondary flux linkage is previously known ψ_2 , then the reference thrust F_e^* and flux ψ_1^* can be illustrated as

$$F_e^* = \frac{3}{2}\frac{\pi}{\tau\sigma}\left(\psi_2 \times \psi_1^*\right) \tag{19}$$

$$\psi_1^* = \psi_1^* \exp\left(j.\angle\psi_1^*\right) \tag{20}$$

$$\angle\psi_1^* = \angle\psi_1 + arcsin\left(\frac{2\tau\sigma F_e^*}{3\pi\psi_1^*\psi_1}\right) \tag{21}$$

First, the cost function J is evaluated for each possible voltage vector ($V_0 - V_7$). The vector that minimizes the cost function is then selected and applied during the next sampling interval.

IV. Integral Sliding Mode Surface Based Super-Twisting Control for Speed Control of The LIM Under FS-MPFC

The speed control loop of the LIM based on integral sliding mode surface under super-twisting control with FS-MPFC is designed. The goal is to control the speed v_r^* of the LIM drive system to track a reference signal, the error of the linear speed of LIM can be v_r^* defined as

$$e = v_r^* - v_r \tag{22}$$

Subsequently, the integral sliding mode surface is chosen to reduce the steady state error of the linear speed of LIM, which can be used to design the super-twisting control method and written as

$$s = e + c\int e\, dt \tag{23}$$

where c>0 is the design constant. The control objective is to force the sliding variable s to zero in finite time. Once s=0, the dynamics are governed by $\dot{s} = 0$, which implies $\dot{e} = -ce$, ensuring exponential convergence of the error e to zero. By taking the derivative of (13), which described as

$$\dot{s} = \dot{e} + ce \tag{24}$$

From the LIM mechanical equations, the derivative of the actual speed is given by:

$$\dot{v}_r = B_n F_e + Z_n F_l + M_n v_r \tag{25}$$

where G is the total mass, H the viscous coefficient of LIM, and M_n=-H/G and B_n=-Z_n=$(JG)^{-1}$ are dissimilar coefficients based on nominal situation, individually. The mechanical dynamics of the LIM under load disturbance is revised as

$$\dot{v}_r = (B_n + \Delta B)F_e + (D_n + \Delta Z)F_l + (\text{M}_n + \Delta A)v_r \tag{26}$$

$$\dot{v}_r = B_n F_e + \Delta d \tag{18}$$

Unlike conventional super-twisting control, which typically uses the speed error as the sliding surface, this paper improves the design by adopting an integral sliding mode surface (ISMS), as defined in (23). Consequently, the control law for the proposed ISMC-STC is designed as follows:

$$\begin{aligned} u &= -k\left|s\right|^{1/2} sign(s) + \sigma \\ \dot{\sigma} &= -k_1 s - k_2 sign(s) \end{aligned} \tag{27}$$

In the ISMC-STC system $\dot{s} = f - gu$, where: $u = F^*{}_e$, total lumped uncertainty $F(t) = v_r + ce - \Delta d(t)$ and $g = B_n$, which is a known control gain of the close loop system. It is assumed the disturbance $\Delta d(t)$ and its derivative are bounded, so $F(t)$ and $\dot{F}(t)$ are bounded: $F(t) \le \text{F}$ and $\dot{F}(t) \le L$ for some known constants F, L >0. Therefore, the final control law can be described as

$$\begin{aligned} F_e^{*} &= F_e^* = B_n^{-1}(u_{sta}) \\ u_{sta} &= -k\left|s\right|^{1/2} sign(s) + \sigma \\ \dot{\sigma} &= -k_2 s - k_1 sign(s) \end{aligned} \tag{28}$$

Based on ISMS has been designed in (20) for the speed loop of the LIM drive system. The system state can be reached on a designed sliding mode surface with faster convergence and less chattering by adjusting the control parameters of the ISMS. Moreover, the DTC technique for the LIM system based on the

ISMS is illustrated in Fig. 1.

V. SIMULATION AND ANALYSIS

To validate the superiority and effectiveness of the MPFC-based ISMS-STC method, Section V and VI presents simulation and experimental studies. The control parameters for the three methods are listed in Table I, and the LIM parameters are in Table II. Two different operational scenarios for the LIM are presented below.

Case 1: Start-up and Steady state Behavior

The performance of the ISMS-STC+MPFC, STC+MPFC, and PI-MPFC controllers is evaluated under a common test scenario involving a startup with a braking under load of 130 N and a speed reference change from 0 to 11 m/s, as shown in Fig. 2. Analysis of the speed behavior in Fig. 2(a) reveals that the proposed ISMS-STC+MPFC method achieves a faster transient behavior with superior reference tracking and quicker convergence than the other two methods. Furthermore, the thrust behavior in Fig. 2(b) demonstrates that the ISMS-STC+MPFC controller not only reaches a steady-state condition more rapidly but also maintains it with the smallest thrust ripple. Fig.2(c) indicates that the primary flux behavior is nearly identical for all control techniques in this scenario. Finally, the phase current under no-load conditions, shown in Fig. 2(d), confirms a significant advantage for the proposed method, as it operates with a markedly lower peak current compared to the STC+MPFC and PI-MPFC controllers. ***Case 2: Speed and Load Change Behavior***

This subsection evaluates the speed change behavior of the LIM drive system under the ISMS-STC+MPFC, PI-MPFC, and STC+MPFC controllers using a combined scenario of speed and load variation. The test conditions are as follows: a constant load of 70 N is applied as the speed reference is set to 6 m/s from 0 to 8 s, and then increased to 10 m/s from 8 to 15 s. Simultaneously with this speed increase, the load is changed from 70 N to 250 N. As shown in Fig. 3(a), the ISMS-STC+MPFC controller demonstrates a faster behavior in reaching the reference speed and a smaller tracking error compared to the PI-MPFC and STC+MPFC methods. Furthermore, the thrust behavior in Fig. 3(b) confirms that the proposed ISMS-STC+MPFC method exhibits lower thrust ripple than the other two controllers. The primary flux for all techniques, shown in Fig. 3(c), remains nearly identical under these operating conditions. Finally, the Phase-A current results in Fig. 3(d) indicate that the ISMS-STC+MPFC controller drives the current to its rated value more rapidly than the alternative methods. The STC+MPFC controllers using a combined scenario of speed and load variation. The test conditions are as follows: a constant load of 70 N is applied as the speed reference is set to 6 m/s from 0 to 8 s, and then increased to 10 m/s from 8 to 15 s. Simultaneously with this speed increase, the load is changed from 70 N to 250 N.

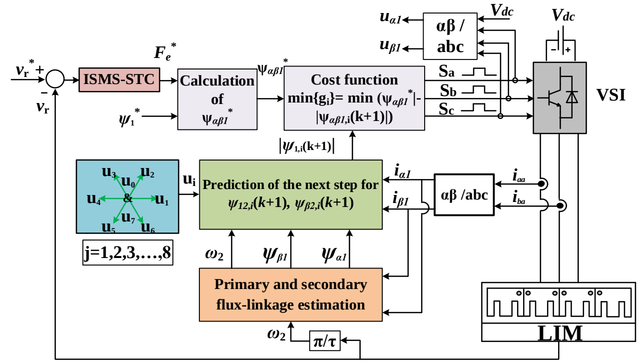

Fig. 1. The FOSMC based FSC-MPFC for the LIM drive system.

TABLE I
THE CONTROL METHODS PARAMETERS

Name	Value
PI-MPFC	300 and 0.1
STC+MPFC	$k = 250,\ k_1 = 30,\ k_2 = 8$
ISMS-STC	$c = 300, k = 250,\ k_1 = 30,\ k_2 = 8$

TABLE II
MAIN PARAMETERS OF THE AIM

Quantity	Symbol	Value	Unit
Rated thrust	F_N	280	N
Rated speed	v_N	11	m/s
Rated current	I_N	22	A
Pole pitch	τ	0.1485	m
Primary length	l_s	1.3087	m
Secondary resistance	R_b	2.4	Ω
Primary leakage inductance	L_{la}	0.0114	H
Primary resistance	R_a	1	Ω

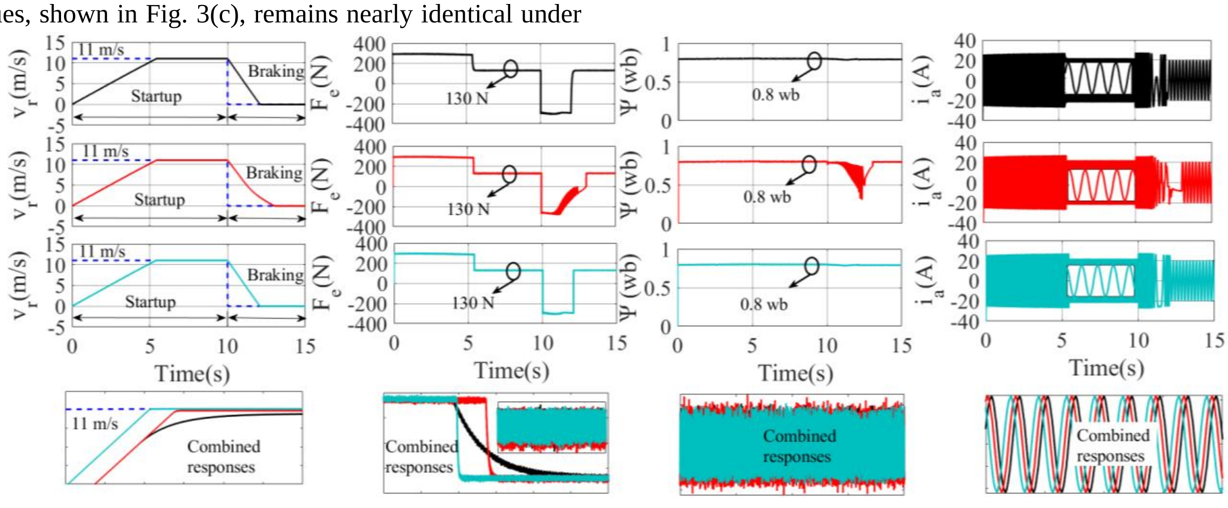

(a) (b) (c) (d)

Fig. 2. The startup and braking profiles for MPFC+PI, MPFC+STC, and MPFC+ISM-STC of the AIM under 11 m/s speed with 130 N load change from top to bottom, respectively.

979-8-3315-8138-1

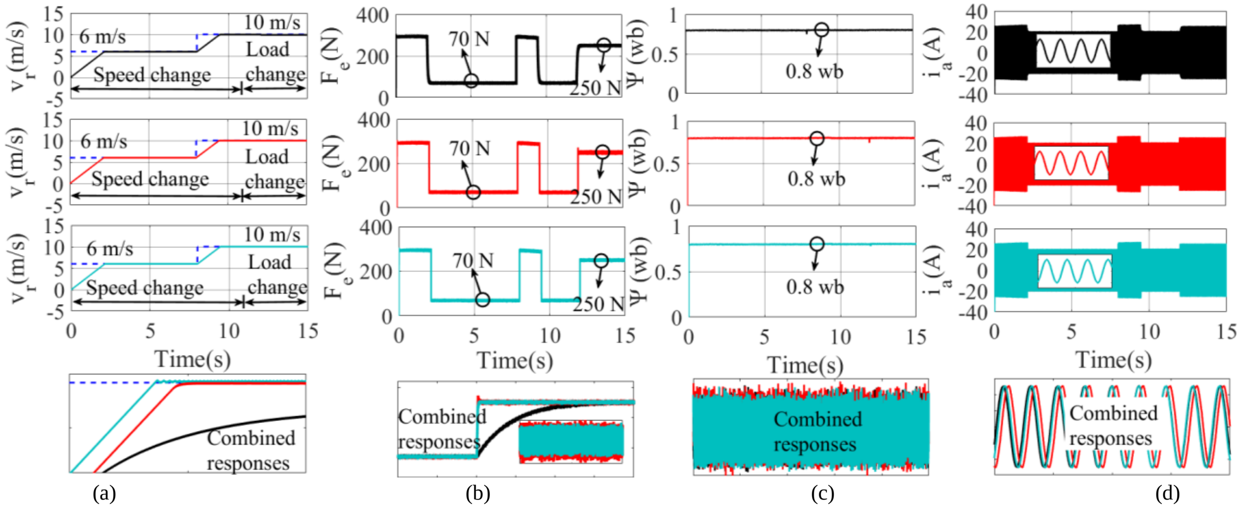

Fig. 3. The startup and braking profiles for MPFC+PI, MPFC+STC, and MPFC+ISM-STC of the AIM under 11 m/s speed with 130 N load change from top to bottom, respectively.

VI. Conclusions

This article presents a novel control strategy that integrates an integral sliding mode surface-based super-twisting control (ISMS-STC) for speed regulation with a finite set-model predictive flux control (FS-MPFC). The FS-MPFC simplifies traditional designs of MPC by eliminating the need for a weighting factor in its cost function. Simulation and experimental results demonstrate that the combined ISMS-STC+MPFC method achieves a quicker dynamic behavior, lesser steady-state error, and reduced thrust and flux ripples compared to common STC+MPFC and PI-MPFC methods. These improvements effectively lower noise and vibration in the LIM drive system. The stability of the proposed ISMS-STC is proven using the Lyapunov theorem, and its effectiveness is comprehensively validated under various operating conditions, including startup, speed variation, and load variation.

References

[1] I. Boldea, L. Tutelea, W. Xu, and M. Pucci, “Linear electric machines, drives, and MAGLEVs: an overview,” *IEEE Trans. Ind. Electron*., vol. 65, no. 9, pp. 7504-7515, Sept. 2018.

[2] Y. Guo, W. Xu, J. Ge, H. Xiao, Y. Tang and Y. Shangguan, "A DSVM-Based MPC Strategy With Magnetizing Inductance Online Identification Method for Thrust Ripple Suppression in Linear Induction Machine," *IEEE Trans. Power Electron*, vol. 40, no. 8, pp. 10746-10757, Aug. 2025.

[3] Y. Guo, W. Xu, J. Ge, Y. Shangguan, H. Xiao and Y. Tang, "A Positive- and Negative-Sequence Equivalent Circuit Model for Linear Induction Machine Adapted to Urban Rail Transit," *IEEE Trans. Transport. Electrific*., vol. 11, no. 4, pp. 9630-9641, Aug. 2025.

[4] W. Xu, J. G. Zhu, S. Member, and Y. Zhang, “Equivalent circuits for single-sided linear induction motors,” *IEEE Trans. on Ind. Appl.* vol. 46, no.6, pp. 2410–2423, 2010.

[5] I. Boldea, *Linear Electric Machines Drives and Maglevs Handbook*. Boca Raton, FL, USA: CRC Press, 2013.

[6] M. M. Ali, W. Xu, M. F. Elmorshedy, S. A. Hamad, A. K. Junejo and M. Ismail, ‘‘Improved Drive Performance of Linear Induction Machine Based on Direct Thrust Control and Sliding Mode Control with Extended State Observer Applied for Linear Metro,” *in Proc. 13th Int. Sym. on Linear Drives for Ind. Appl. (LDIA)*, Wuhan, China, 2021, pp. 1-6.

[7] F. Alonge, M. Cirrincione, M. Pucci, and A. Sferlazza, “Input-output feedback linearization control with on-line MRAS-based inductor resistance estimation of linear induction motors including the dynamic end effects,” *IEEE Trans. Ind. Appl*., vol. 52, no. 1, pp. 254–266, Feb.

[8] H. Karimi, S. Vaez-zadeh, and F. R. Salmasi, “Combined vector and direct thrust control of linear induction motors with end effect compensation,” *IEEE Trans. Energy Convers.*, vol. 31, no. 1, pp. 196-205, Mar. 2016.

[9] W. Xu, X. Xiao, G. Du, D. Hu, and J. Zou, “Comprehensive efficiency optimization of linear induction motors for urban transit,” *IEEE Trans. on Veh. Technol.*, vol. 69, no. 1, pp. 131-139, Jan. 2020.

[10] A. K. Junejo, Y. Tang, W. Xu, J. Ge and M. R. Islam, "Adaptive Fast Super-Twisting Sliding Mode Direct Thrust Control for Linear Induction Machine Adapted to Linear Metro," *IEEE Trans. Transport. Electrific*., Early Access.

[11] A. K. Junejo, W. Xu, Y. Tang, H. Xiao, K. Wang and M. M. Ismail, "Robust Adaptive Terminal Reaching Law-Based Sliding Mode Direct Thrust Control for LIM Adapted to Urban Transportation," *IEEE Trans. Transport. Electrific*, vol. 11, no. 2, pp. 5781-5792, April 2025.

[12] W. Xu *et al*., "Discrete Space Vector Modulation-Based MPCC With Inductance Identification for Thrust Ripple Suppression in Linear Induction Machine," *IEEE Trans. Power Electron*, vol. 39, no. 10, pp. 12883-12893, Oct. 2024.

[13] Q. G. Ke Wang, Y. Li, and L. Shi, “A novel switching scheme for direct thrust control of LIM with reduction of thrust ripple,” *in Proc. Int. Con. Elect. Mach. Syst.*, pp. 1491–1494, 2010.

[14] N. Abdelfatah and G. Brahim, “A novel lithium-ion battery autonomous strategy improvement based on SVM-DTC for urban electric vehicle under several speeds tests,” *Majlesi Journal of Electrical Engineering*, vol. 5, no. 4, Dec. 2011.

[15] A. K. Junejo, W. Xu, Y. Tang, K. Liao, H. Xiao and Y. Li, "Enhanced Cascade Sliding Mode Direct Thrust Control for Linear Induction Machine Based on Linear Metro," *IEEE Trans. Power Electron*, vol. 39, no. 9, pp. 11517-11531, Sept. 2024.

[16] Y. Sun, Z. He, J. Xu, F. Li and D. Zhang, “Cooperative Model Predictive Levitation Control for Two-Points Electromagnetic Levitation System of High-Speed Maglev Vehicle,” *IEEE Trans. Intell. Veh*., Early Access, pp. 1-12, Nov. 2023.

[17] A. A. Ahmed, B. K. Koh, and Y. Il Lee, “A comparison of finite control set and continuous control set model predictive control schemes for speed control of induction motors,” *IEEE Trans. Ind. Informat*., vol. 14, no. 4, pp. 1334–1346, Apr. 2018.

[18] Y. Zhang, J. Jin and L. Huang, “Model-Free Predictive Current Control of PMSM Drives Based on Extended State Observer Using Ultralocal Model,” *IEEE Trans. Ind. Electron.*, vol. 68, no. 2, pp. 993-1003, Feb. 2021.

[19] W. Xu, Y. Tang, D. Dong, X. Xiao, E. E. M. Rashad and A. K. Junejo, "Optimal Reference Primary Flux Based Model Predictive Control of Linear Induction Machine With MTPA and Field-Weakening Operations for Urban Transit," *IEEE Trans. Ind. Appl*., vol. 58, no. 4, pp. 4708-4721, July-Aug. 2022.

[20] S. A. Bukhari, W. Xu, M. F. Elmorshedy, A. K. Junejo and S. A. Hamad, “Upgraded Limited-Step Predictive Current Control Strategy for Linear Induction Machine based on Linear Metro,” *in Proc. 13th Int. Sym. on Linear Drives for Ind. Appl. (LDIA)*, Wuhan, China, 2021, pp. 1-6.

[21] M. M. Ali, W. Xu, A. K. Junejo, M. F. Elmorshedy and Y. Tang, "One New Super-Twisting Sliding Mode Direct Thrust Control for Linear Induction Machine Based on Linear Metro," *IEEE Trans. Power Electron*., vol. 37, no. 1, pp. 795-805, Jan. 2022.

979-8-3315-8138-1